ChemComm

A core-substituted naphthalene diimide-based supramolecular triangle and its self-assembly into nanostructures

Journal:	*ChemComm*
Manuscript ID	CC-COM-02-2025-000943.R1
Article Type:	Communication

ChemComm

COMMUNICATION

A core-substituted naphthalene diimide-based supramolecular triangle and its self-assembly into nanostructures

Received 00th January 20xx,
Accepted 00th January 20xx

DOI: 10.1039/x0xx00000x

Samantha T. Aragon,[a] Edgar U. Lopez-Torres,[b] Franchesca C. Tinacba,[a] Camille J. Kwan,[a] Joshua J. Do,[a] Rosanna Jees,[a] Daniella S.A. Unpingco,[a] Daniel J. Wherritt,[c] Jon R. Parquette*[b], Peter J. Cragg *[d] and Erendra Manandhar *[a]

A core-substituted naphthalene diimide (1) was self-assembled with $(Et_3P)_2Pt{\cdot}2TfO$ to a triangular structure (2) whereas an equilibrium mixture of triangular and dimer or tetramer was obtained with Pd(dppp)·2TfO and Pt(dppp)·2TfO. The triangular structure for 2 was supported theoretically by PM6 calculations and fully characterized by NMR spectroscopy and mass spectrometry. Complex 2, as compared to 1, shows a variable UV-Vis absorption and fluorescence as a function of solvent and is easily reducible during cyclic voltammetry. TEM and AFM imaging showed that 2 further self-assembles into nanostructures.

Since the first reports on palladium and platinum-based macrocycles in the early 1990s by Fujita and Stang et al., a plethora of 2D metallocycles and 3D metallocages has been reported including those assembling into triangles, squares, rectangles, cubes, tetrahedra, octahedra and other assemblies.[1-3] These metallosupramolecular structures, owing to their well-defined cavities, offer potential applications in catalysis, sensors, host-guest chemistry, and biomedicine.[4] The ligands and metal centers play crucial roles in the size, shape, and function of these supramolecular structures.[5] Often linear rigid dipyridyl ligands self-assemble into molecular triangles or squares.[6] However, numerous examples with triangles and squares in equilibrium have been reported where there is no clearly favored thermodynamic structure and the ratio between the two changes depending on the solvent, temperature, and counterions.[7-10] This is often the case with the flexible ligands which, owing to entropic effects, can distort their shape favoring smaller structures over the larger structures. Fujita et al. and Sallé et al. also showed that metal centers and their ancillary ligands can influence the equilibrium through electronic and steric effects.[11, 12] Supramolecular coordination complexes (SCCs) can further self-assemble into hierarchical structures via combinations of multiple non-covalent interactions.[13] Functional groups such as alkyl, alkoxy, crown ethers that possess non-covalent interactions such as hydrophobic, hydrophilic, hydrogen bonding, and π-π interactions are introduced as secondary driving forces into SCCs to induce such hierarchical self-assembly.[14] The construction of complex hierarchical structures comparable to biological macromolecules such as proteins is an area of current research interest. A variety of functional materials including metallohydrogels, and amphiphilic nanostructures have been prepared by this approach with wide-ranging applications from catalysis to energy storage, sensing and biomedicine.[15]

Several macrocycles and cages functionalized with naphthalene diimide (NDI) have been reported but are still limited and understudied, in particular, systems based on palladium and platinum.[16] This is in contrast to perylene diimide (PDI), a higher homologue of rylenediimide, as several PDI based macrocycles and cages have been developed by Wurther et al.[9, 17] and others with various applications.[18] Similar to PDI, NDI is electron deficient, and redox active but planar in contrast to bay substituted PDI, which makes it highly amenable to the π-stacking interactions leading to higher order morphologies.[19, 20] Core-substituted naphthalene diimde (cNDI), with one or more substituents in core positions, has tunable electrochemical and optical properties with potential applications in molecular recognition, photoinduced electron transfer and organic solar cells.[21] A few core-substituted and un-substituted NDI-based tetrahedral cages with sensing and catalytic activities were developed by Nitschke et al.[22, 23] and others reported a dipyridyl naphthalene diimide based palladium square and cage.[7, 24, 25] Surprisingly to the best of our knowledge, core-substituted NDI-based metallocycles and their properties have yet to be reported.

[a] Department of Chemistry and Biochemistry, St. Mary's University, San Antonio, TX, US. E-mail: emanandhar1@stmarytx.edu
[b] Department of Chemistry and Biochemistry, Ohio State University, Columbus, OH, US. Parquette.1@osu.edu
[c] Department of Chemistry, University of Texas at San Antonio, San Antonio, US
[d] School of Applied Sciences, University of Brighton, Brighton, UK
p.j.cragg@brighton.ac.uk

†Electronic supplementary information (ESI) available: Detailed experimental procedures and characterization data, ^{1}H NMR, ^{13}C NMR, ^{31}P NMR, 2D NMR, ESI mass spectra, theoretical calculation, AFM/TEM, imaging and cyclic voltammetry are available in the electronic supplementary material.

Herein we present the coordination-driven self-assembly of a core-substituted naphthalene diimide functionalized with pyridinyl phenyl in the 2,6-positions and octyl groups on the imide nitrogens (**1**) with Pt(II) and Pd (II) phosphane triflates [$(Et_3P)_2$Pt·2TfO, Pd(dppp) ·2TfO and Pt(dppp·2TfO, dppp = 1,3-bis(diphenylphosphino)propane, TfO = trifluoromethane sulfonate]. A triangular structure was formed on self-assembly with all three metal triflates as confirmed by NMR and mass spectrometry (Scheme 1). However, a mixture was formed in the case of Pd(dppp)·2TfO and Pt(dppp)·2TfO. Semiempirical calculations indicated the formation of a symmetrical triangular structure for **2** which, on further self-assembly via non-covalent interactions, produces spherical structures as shown by TEM and AFM imaging. A photophysical studies showed that absorption and fluorescence of **2** varies with the solvent. Cyclic voltammetry of **2** showed a two reversible reduction waves, corresponding to anion and dianion, at lower potentials than **1**.

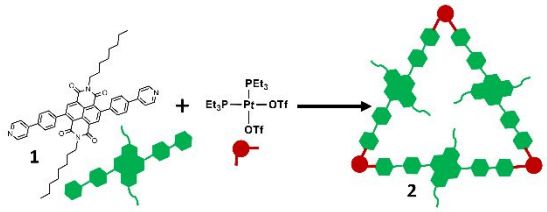

Scheme 1 Self-assembly of supramolecular triangle (**2**).

Ligand **1** was synthesized in 75% yield by a Suzuki coupling between 4-pyridinyl phenyl boronic acid and 2,6-dibromo dioctyl NDI. The latter was prepared by heating 2,6-dibromo NDA with octylamine in acetic acid at 90°C .[26] The stoichiometric reaction of **1** with $(Et_3P)_2$Pt·2TfO in dichoromethane for 48 h at room temperature, followed by slow vapor diffusion of diethyl eher into the reaction mixture, yielded a yellow precipitate of complex **2** in nearly quantitative yield.[1] Similar reactions were carried out with Pd(dppp)·2TfO and Pt(dppp)·2TfO which gave yellow precipitates of dppp-capped Pd(II) and Pt(II) complexes, respectively. All complexes were highly soluble in dichloromethane, with moderate solubility in chloroform, acetone and acetonitrile, and were characterized by ^{1}H, ^{31}P(H) NMR spectroscopy and high-resolution ESI mass spectrometry (ESI†).

The ^{1}H NMR spectrum of **2** for the complex of **1** with $(Et_3P)_2$Pt.2TfO shows only one set of signals with pyridinyl protons $\mathbf{H_a}$ (Δδ = 9.472-8.743), $\mathbf{H_b}$ (Δδ = 7.951-7.649) and phenyl proton $\mathbf{H_c}$ (Δδ = 7.897-7.578) shifted downfield while phenyl proton $\mathbf{H_d}$ (Δδ = 7.847-7.533) and NDI proton $\mathbf{H_e}$ (Δδ = 8.710-8.595) shifted upfield compared to **1** (Fig. 1a). The downfield shift of the pyridinyl protons is a clear indication of the loss of electron density upon coordination to the metal. In agreement with the ^{1}H NMR, the ^{31}P NMR of **2** showed a single peak centered at -4.74 ppm, which is shifted upfield by approximately 13.0 ppm compared to its precursor, [$(Et_3P)_2$Pt.2TfO], which is observed at 8.13 ppm in $CDCl_3$ (Fig. 1b). This upfield shift, together with the single peak in the ^{31}P NMR, confirmed a symmetric phosphorous center in **2**. However, multiple signals were observed in the ^{1}H NMR for dppp-capped Pd(II) and Pt(II) complexes with similar changes in the chemical shift from **1**. Similarly, the ^{31}P NMR of dppp-capped Pd(II) showed two peaks at 6.411 and 5.972 ppm while dppp-capped Pt(II) showed two peaks at -15.130 and -15.450 ppm indicating multiple species in solution. The study of ^{1}H and ^{31}P NMR in various solvents also confirmed only one species in **2** and multiple species in dppp-capped Pd(II) and Pt(II) complexes (Fig. S7-10, ESI†). Furthermore, a single set of signals was observed in the ^{1}H DOSY NMR of **2** with a diffusion coefficient of $D = 4.25 \times 10^{-10}$ m^{2}s^{-1}, supporting the presence of only one discrete self-assembled species exists in solution, while multiple set of signals were observed in DOSY spectra of other complexes further supporting the presence of multiple species (Fig. S36-38, ESI†). This showed that in addition to ligand flexibility, substituents at metal plays a crucial role in the self-assembly. A similar behavior was reported previously with an equilibrium between triangular and square structures in solution where one species is generally isolated over another via crystallization or/and precipitation.[7, 8]

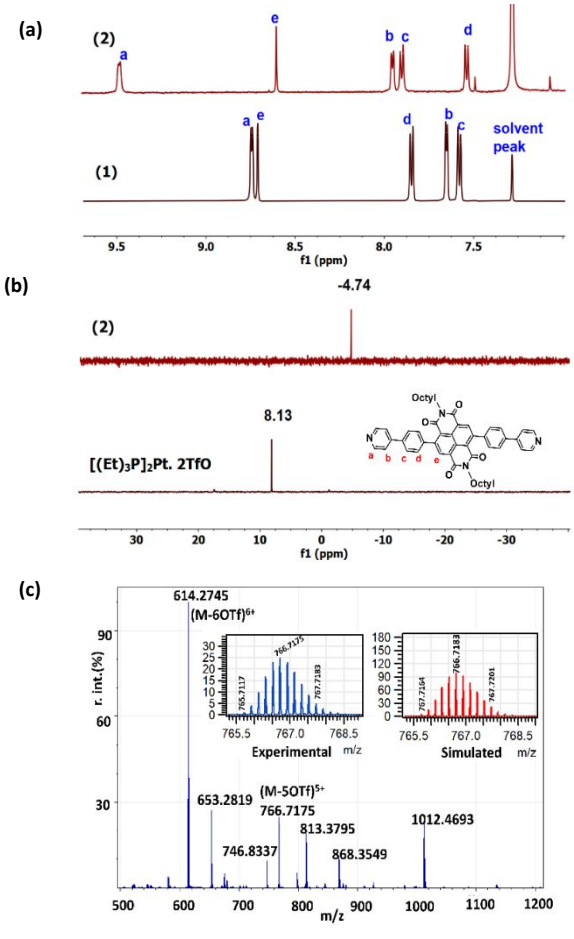

Fig. 1 (a) Partial ^{1}H NMR (aromatic region) stack plot of **1** and **2** in $CDCl_3$. (b) ^{31}P stack plot of $(Et_3P)_2$Pt.2TfO and **2** in $CHCl_3$ (c) ESI-MS spectra of **2**.

Electrospray ionization mass spectrometry (ESI-MS) of **2** identified masses consistent with the formation of the proposed triangular structure. A solution of complex **2** in DMSO at nanomolar concertation showed tetra-, penta- and hexacationic peaks at m/z 995.6360, 766.7175 and 614.2745 corresponding to consecutive loss of four to six triflate ions

respectively (Fig. 1c). Peaks were isotopically resolved and well matched with corresponding theoretical distribution patterns. Other peaks at m/z 813.3795, and 1012.4693 observed in the mass spectrum of **2** could be attributed to fragmentation due to in-source collision-induced dissociation. In addition to peaks corresponding to a triangular structure, there is a peak for the trication, with the loss of three triflate ions, centered at m/z 868.3482 indicating the presence of a dimeric structure at high dilution. Similar to **2**, the mass spectrum of the dppp-capped Pt(II) complex showed a triangular structure as the major species with a tetramer (square structure) as the minor species in the solution. By contrast, dppp:-capped Pd(II) complex only showed peaks for a dimeric structure in the mass spectrum as palladium complexes are usually less stable and dissociated under ESI condition (Fig. S11-13, ESI†).[17]

The photophysical properties of **1** and **2** were investigated by UV-Vis absorption and fluorescence spectroscopy in various solvents. The absorption spectrum of **2** (20μM) in acetonitrile, similarly to **1**, exhibited a strong absorption band at ~285 nm, two prominent absorption bands at 360 and 380 nm arising from the π-π* transitions polarized along the long axis of NDI and a red shifted broad band at ~415 nm assigned to weak intramolecular photoinduced charge transfer from pyridinyl phenyl moieties to NDI core.[19] The absorption spectrum of **2** is blue shifted by ~2 nm in acetonitrile and acetone, compared to chloroform, indicating possible aggregation (Fig. S19-20, ESI†). This is supported by the concentration dependent behavior of **2** in acetonitrile which showed a ~20 nm blue shift of band at ~285 nm on dilution from 2.5 to 25 μM. A temperature dependence study showed a blue shift and an increase in intensity of bands at ~285 nm, 360 and 378 nm with decrease in base line scattering above 450 nm indicating disaggregation (Fig. S21-22, ESI†). Fluorescence of **1** (20μM) is weak, possibly due to intramolecular rotation of the pyridinyl phenyl unit with respect to the naphthalene lowering the radiative quantum yield.[27, 28] By way of contrast, **2**, on excitation at 410 nm, shows variable emissions in different solvents with slightly higher emission in chloroform and DMF. A lower emission of **2** in acetonitrile and acetone could be due to aggregation caused quenching (ACQ) phenomenon supporting its aggregation behavior (Fig. S19 ESI†). Additionally, redox properties of **1** and **2** were studied by cyclic voltammetry in dichloromethane with ferrocene as the internal standard. Two reversible reduction waves were observed corresponding to the formation of radical anion and dianion with **1** ($E_{1/2}$ = -0.87 and -1.25 V vs Fc/Fc+) at slightly negative than **2** ($E_{1/2}$ -0.82 and -1.18 V vs Fc/Fc+) indicating **2** is more reducible than **1.**[29] This is considerable as **2** becomes more electron deficient after coordination with the platinum ions (Fig. S24, ESI†).

All attempts to grow crystals suitable for single crystal X-ray diffraction studies were not successful. Therefore, *in silico* simulations were performed in order to propose a structure of **2** as well as structure and frontier molecular orbital energies of **1**.[30, 31] As expected, trimer **2** forms a stable symmetric triangular structure in agreement with mass spectrometric data, (Fig. 2a). Platinum ions and the NDI core formed the corners and sides of the triangle, respectively, with the NDI core opposite to the platinum corner with a distance of 2.56 nm. The sides of triangle (Pt to Pt) are slightly bent outward with distance of 2.58 nm while neighbouring NDI cores are 1.87 nm apart. All octyl groups of NDI cores are pointed outside the cavity while pyridine, phenyl and NDI core are almost orthogonal to each other as in **1**. The interior angle between the adjacent ligands of the triangle is found to be around 98° deviating from the expected 90° for a square planer geometry around the platinum (II) ion. The effect of triflate anions on the structure of **1** as well as **2** is found to be negligible (Fig. S15-16, ESI†). The HOMO and LUMO of **1** showed that LUMO was mainly associated with the naphthalimide moiety whereas the HOMO was mostly localized along the pyridyl axis. The HOMO-LUMO energy gap for **1** was calculated to be -2.97 eV which equates to an absorbance at 417 nm and is in excellent agreement with the experimentally determined value of 415 nm (Fig. S14, ESI†).

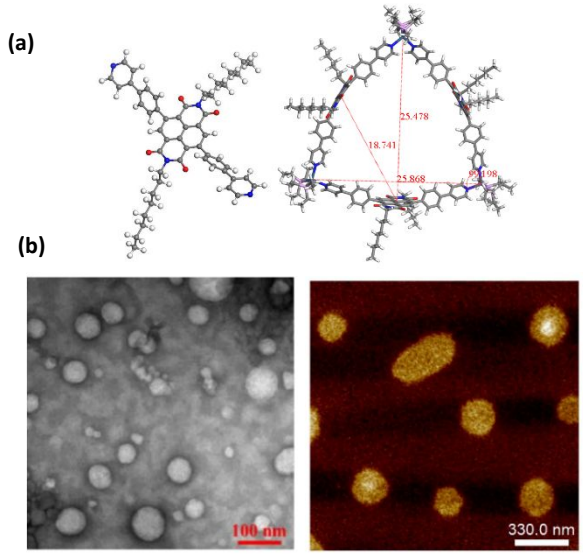

Fig. 2 (a) DFT and geometry optimized model of **1** and **2**. (b) TEM and Peak Force Tapping AFM images of **2** (100 **μM**) in CH_3CN after 24 h on freshly cleaved mica.

Inspired by the UV-Vis results and strong tendency of NDI to engage in π–π interactions, imaging studies were performed to investigate the assembly characteristics of **2** as a function of solvent. After screening several solvent systems, acetonitrile was selected because it facilitated the formation of a well-ordered nanostructure. Transmission electron microscopy (TEM) of **2** (100 μM), imaged in acetonitrile after 24 h, revealed an array of spherical particles with diameters ranging from 10–120 nm (Fig.2b). Time-dependent UV-Vis spectroscopy revealed evidence of characteristic π–π stacking of the NDI chromophores (Fig. S22, ESI†).[19] A decrease in absorption intensity suggested the presence of π–π interactions, often associated with the formation of nanospheres.[32] Additionally, after 24 hours, baseline scattering became apparent, which may be attributed to the formation of larger aggregates. These changes were also observable in the vial (Fig. S23, ESI†). The spherical structures were likely formed by the further self-assembly of **2** via combination of multiple non-covalent

interactions such as π–π, ionic and solvophobic effects. Varying sizes of spherical structures could result from different numbers of triangular units stacked in each spherical structure while further aggregation of these individual spheres leads to larger structures. The formation of spherical structures was further supported by AFM where diameters were found to range from 120–250 nm, with an average size larger than that observed by TEM. Additional AFM images taken at higher concentration (5.0 mM) appeared more consistent and closely resemble the TEM images with sectional analysis indicating a uniform size of ~70-80 nm (Fig. S18, ESI†). To further confirm the size of the particles, a dynamic light scattering (DLS) was carried out at a concentration 0.5 mM but did not result in any significant scattering, however, concentrated solution (5.0 mM) showed Z average of 4691-5397 nm, which is considerable, due to aggregation at higher concentration (Fig. S23, ESI†).

In summary, a new core-substituted NDI-based supramolecular triangle (**2**) was successfully prepared via coordination driven self-assembly of **1** with $(Et_3P)_2Pt{\cdot}2TfO$ while an equilibrium mixture was obtained with Pd(dppp)·2TfO and Pt(dppp)·2TfO highlighting the steric/electronic effect of ancillary ligands of metals. The formation of a triangular structure is confirmed by various analytic techniques and further supported by PM6 semiempirical calculations. Complex **2** showed a variable absorption and emission as a function of solvent and undergoes reversible reduction waves at lower potential than **1**. Moreover, TEM and AFM imaging showed that **2** undergoes further self-assembly via multiple non-covalent interactions to form nanostructures. This study provides an exciting route to study the photophysical properties and hierarchical self-assembly behaviors of core-substituted NDI-based self-assembled metallocycles and cages in the future.

EM gratefully thanks the WelchGrant, SPARC and URISE of St. Mary's University, Dr. Wendell P. Griffith for Mass Spectrometry and NMR facility at University of Texas at San Antonio. We also acknowledge the National Science Foundation (CHE-2106924, JRP) and TEM/AFM facility at the Ohio State University.

Conflicts of interest

There are no conflicts to declare.

Data availability

Detailed experimental procedures and characterization data, ^{1}H NMR, ^{13}C NMR, ^{31}P NMR, 2D NMR, ESI mass spectra, theoretical calculation, AFM/TEM, imaging and cyclic voltammetry are available in the electronic supplementary information (ESI).

Notes and references

1.P. J. Stang and D. H. Cao, *Journal of the American Chemical Society*, 1994, **116**, 4981-4982.
2.M. Fujita, J. Yazaki and K. Ogura, *Journal of the American Chemical Society*, 1990, **112**, 5645-5647.
3.T. R. Cook and P. J. Stang, *Chemical Reviews*, 2015, **115**, 7001-7045.
4.C. Yin, J. Du, B. Olenyuk, P. J. Stang and Y. Sun, *Inorganics*, 2023, **11**, 54.
5.S. Verma, V. Vajpayee, S. M. Lee, H. J. Jung, H. Kim and K.-W. Chi, *Inorganica Chimica Acta*, 2012, **387**, 435-440.
6.D. Zhang, *Dyes and Pigments*, 2016, **127**, 128-132.
7.K. Aoki, K. Otsubo and H. Kitagawa, *CrystEngComm*, 2021, **23**, 7691-7697.
8.S. Goeb, S. Bivaud, P. I. Dron, J.-Y. Balandier, M. Chas and M. Sallé, *Chemical Communications*, 2012, **48**, 3106-3108.
9.A. Sautter, D. G. Schmid, G. Jung and F. Würthner, *Journal of the American Chemical Society*, 2001, **123**, 5424-5430.
10.G. Gupta, A. Das, K. C. Park, A. Tron, H. Kim, J. Mun, N. Mandal, K.-W. Chi and C. Y. Lee, *Inorganic Chemistry*, 2017, **56**, 4615-4621.
11.M. Fujita, O. Sasaki, T. Mitsuhashi, T. Fujita, J. Yazaki, K. Yamaguchi and K. Ogura, *Chemical Communications*, 1996, 1535-1536.
12.J.-Y. Balandier, M. Chas, S. Goeb, P. I. Dron, D. Rondeau, A. Belyasmine, N. Gallego and M. Sallé, *New Journal of Chemistry*, 2011, **35**, 165-168.
13.Z. Zhang, Q. Bai, E. Manandhar, Y. Zeng, T. Wu, M. Wang, L.-Y. Yao, G. R. Newkome, P. Wang and T.-Z. Xie, *Chemical Science*, 2022, **13**, 5999-6007.
14.S. Datta, M. L. Saha and P. J. Stang, *Accounts of Chemical Research*, 2018, **51**, 2047-2063.
15.G.-Y. Wu, C. Liang, Y.-X. Hu, X.-Q. Wang, G.-Q. Yin and Z. Lu, *RSC Advances*, 2021, **11**, 1187-1193.
16.Q.-H. Ling, J.-L. Zhu, Y. Qin and L. Xu, *Materials Chemistry Frontiers*, 2020, **4**, 3176-3189.
17.F. Würthner, A. Sautter, D. Schmid and P. J. A. Weber, *Chemistry – A European Journal*, 2001, **7**, 894-902.
18.R. Li, T. Yang, X. Peng, Q. Feng, Y. Hou, J. Zhu, D. Chu, X. Duan, Y. Zhang and M. Zhang, *Nano-Micro Letters*, 2024, **16**, 226.
19.H. Shao, J. Seifert, N. C. Romano, M. Gao, J. J. Helmus, C. P. Jaroniec, D. A. Modarelli and J. R. Parquette, *Angewandte Chemie International Edition*, 2010, **49**, 7688-7691.
20.S. Tu, S. H. Kim, J. Joseph, D. A. Modarelli and J. R. Parquette, *Journal of the American Chemical Society*, 2011, **133**, 19125-19130.
21.N. Sakai, J. Mareda, E. Vauthey and S. Matile, *Chemical Communications*, 2010, **46**, 4225-4237.
22.Z. Lu, T. K. Ronson and J. R. Nitschke, *Chemical Science*, 2020, **11**, 1097-1101.
23.Z. Lu, R. Lavendomme, O. Burghaus and J. R. Nitschke, *Angewandte Chemie International Edition*, 2019, **58**, 9073-9077.
24.S. Ganta and D. K. Chand, *Inorganic Chemistry*, 2018, **57**, 3634-3645.
25.M. A. Gordillo, P. A. Benavides and S. Saha, *Crystal Growth & Design*, 2019, **19**, 6017-6022.
26.Y. Yao, S. Chakraborty, S. Zhu, K. J. Endres, T.-Z. Xie, W. Hong, E. Manandhar, C. N. Moorefield, C. Wesdemiotis and G. R. Newkome, *Chemical Communications*, 2017, **53**, 8038-8041.
27.S. Chopin, F. Chaignon, E. Blart and F. Odobel, *Journal of Materials Chemistry*, 2007, **17**, 4139-4146.
28.S. V. Bhosale, M. B. Kalyankar, S. V. Bhosale, S. J. Langford, E. F. Reid and C. F. Hogan, *New Journal of Chemistry*, 2009, **33**, 2409-2413.
29.J. Shukla and P. Mukhopadhyay, *European Journal of Organic Chemistry*, 2019, **2019**, 7770-7786.
30.Spartan '24, *Journal*, Wavefunction Inc. Irvine, CA 92612, USA.
31.M. R. Sambrook, J. C. Vincent, J. A. Ede, I. A. Gass and P. J. Cragg, *RSC Advances*, 2017, **7**, 38069-38076.
32.P. Jana, S. K. Maity, S. Bera, P. K. Ghorai and D. Haldar, *CrystEngComm*, 2013, **15**, 2512-2518.

Detailed experimental procedures and characterization data, ^{1}H NMR, ^{13}C NMR, ^{31}P NMR, 2D NMR, ESI mass spectra, theoretical calculation, AFM/TEM, imaging and cyclic voltammetry are available in the electronic supplementary material.